Tuning electronic structure and luminescence of self-activated $Ca_3WO_5Cl_2$ phosphors by hydrostatic pressure

QUANWANG NIU[1,2], YUNPENG ZHANG[1], XIANGFU WANG[1,2,*], XIAOHONG YAN[1,2]
[1]*College of Electronic and Optical Engineering & College of Flexible Electronics (Future Technology), Nanjing University of Posts and Telecommunications, Nanjing, 210023, China*
[2]*The Key Laboratory of Radio and Micro-Nano Electronics of Jiangsu Province, Nanjing, 210023, China*

This paper mainly focuses on the electronic structure and optical properties of self-activated $Ca_3WO_5Cl_2$ phosphors under pressure using the first-principles based on density functional theory. The calculated results indicated that the band gap of $Ca_3WO_5Cl_2$ drops from 3.409 eV to 2.715 eV with the increase of pressure from 0 GPa to 100 GPa. Furthermore, it was found that the absorption coefficients of $Ca_3WO_5Cl_2$ in the ultraviolet region were gradually greater with the increase of pressure according to the comprehensive observation of their optical properties in the energy range of 0 eV-60 eV.

(Received July 24, 2023; accepted December 4, 2023)

Keywords: Density functional theory, Self-activated phosphor, High pressure, Electronic structure, Optical properties

1. Introduction

Self-activated phosphors, known as non-doped phosphors, offer several advantages over doped luminophores, including structural stability, wide emission wavelength range, low preparation temperature, and minimal environmental impact [1-3]. As a result, they have gained significant attention from researchers. Among them, tungstates have emerged as promising self-activated luminescent materials due to their excellent luminescence efficiency and chemical stability, leading to their applications in light-emitting diodes [4-7], field-emission displays [8], optical thermometers [9], and anti-counterfeit markers [10, 11]. A notable example of self-activated tungstate phosphors is $Ca_3WO_5Cl_2$ [12]. When excited by ultraviolet (UV) light, pure $Ca_3WO_5Cl_2$ exhibits blue-green emission [13], which can be attributed to the charge transfer (CT) transition between O-2p and W-5d orbitals.

Pressure can induce changes in the internal atomic spacings and cell shapes of tungstates, potentially resulting in phase transitions. Several studies have investigated the effects of pressure on tungstate materials. For instance, Cai used first-principles calculations to demonstrate that the peak position of the imaginary part of the dielectric function and the edge of the absorption band of $MnWO_4$ are affected by applied pressure [14]. Ablett applied pressure to $PbWO_4$ and observed a phase transition from $PbWO_4$-I to $PbWO_4$-III near 7 GPa [15]. Mahlik investigated the quenching of red luminescence in a single crystal of $KY(WO_4)_2$ doped with Pr^{3+} under high pressure [16]. These studies indicate that the photoelectric properties of tungstates can be effectively modulated by pressure. However, the electronic and optical properties of $Ca_3WO_5Cl_2$ under high pressure have received limited attention and require further investigation.

In this paper, we present a comprehensive study of the electronic structure and optical properties of $Ca_3WO_5Cl_2$ under different hydrostatic pressures (ranging from 0 to 100 GPa with a 10 GPa interval) using first-principles calculations based on density functional theory (DFT). The analysis encompasses lattice parameters, band structure, density of states, charge density difference, dielectric function, absorption coefficient, reflectivity, and complex refractive index. The calculated optical properties reveal a blue shift in the absorption spectra of $Ca_3WO_5Cl_2$ towards higher energy in the UV region, accompanied by an increase in the absorption coefficients with increasing pressure. Consequently, $Ca_3WO_5Cl_2$ holds promise as a material for the development of pressure-modulated UV filters. The findings of this research provide valuable theoretical insights for enhancing the optical properties of self-activated tungstate materials and expanding their applications.

2. Method of calculation

The calculations were carried out using the plane-wave pseudopotential method [17-21]. The ion-electron interactions were treated by the ultrasoft pseudopotential, and the exchange correlation energy of the electron interactions was treated by the Perdew-Burke-Ernzerhof (PBE) method under the

generalised gradient approximation (GGA) [22-24]. The integral calculation of the system in the Brillouin zone was performed using the Monkhorst-Pack scheme [25], with the K-point grid set to 3 × 6 × 3 for $Ca_3WO_5Cl_2$. The plane wave cutoff energy was set to 380 eV. The cell volume, atomic positions and cell shape were fully relaxed before the calculation to obtain the stable structure of the system. The method used to optimise the model structure is Broyden-Fletcher-Goldfarb-Shanno (BFGS) [26, 27]. During the optimisation iteration, the maximum displacement is 5.0×10^{-4} Å, the maximum internal stress is 0.02 GPa, the maximum interatomic interaction force is 0.01 eV/Å, and the total energy of the structure converges to 5.0×10^{-6} eV/atom. The valence electron states of each element involved in the calculations are Ca-$3s^2 3p^6 4s^2$, W-$5s^2 5p^6 5d^4 6s^2$, O-$2s^2 2p^4$, Cl-$3s^2 3p^5$.

3. Results and discussions

The crystal structure of $Ca_3WO_5Cl_2$ is depicted in Fig. 1(a), which belongs to the orthorhombic crystal system with the space group Pnma (62). In this structure, the W^{6+} ion occupies the centre of a distorted octahedral arrangement formed by five O^{2-} ions and one Cl^- ion. The W-O bond distances range from 1.78 to 1.95 Å, while the W-Cl bond distance is longer, about 3.26 Å [28]. To ensure the reliability of our results, full relaxation of the unit cell was performed. The optimised lattice parameters of $Ca_3WO_5Cl_2$ are presented in Table 1 and compared with values reported in the literature.

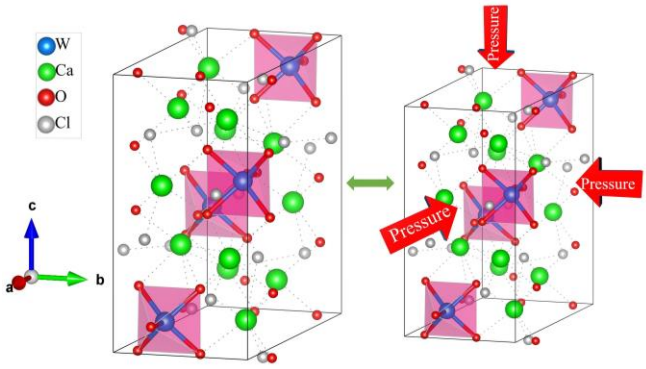

Fig. 1. The crystal structure of $Ca_3WO_5Cl_2$ and a schematic representation of the hydrostatic pressure exerted on the crystal (color online)

Fig. 2 illustrates the significant changes in the lattice parameters and volumes of $Ca_3WO_5Cl_2$ under hydrostatic pressure ranging from 0 to 100 GPa with an interval of 10 GPa. As shown in Fig. 2(a), the lattice parameters of $Ca_3WO_5Cl_2$ gradually decrease as the pressure increases up to 100 GPa. Furthermore, Fig. 2(b) demonstrates that the cell volume of $Ca_3WO_5Cl_2$ decreases with increasing hydrostatic pressure, indicating a reduction in atomic spacing under pressure.

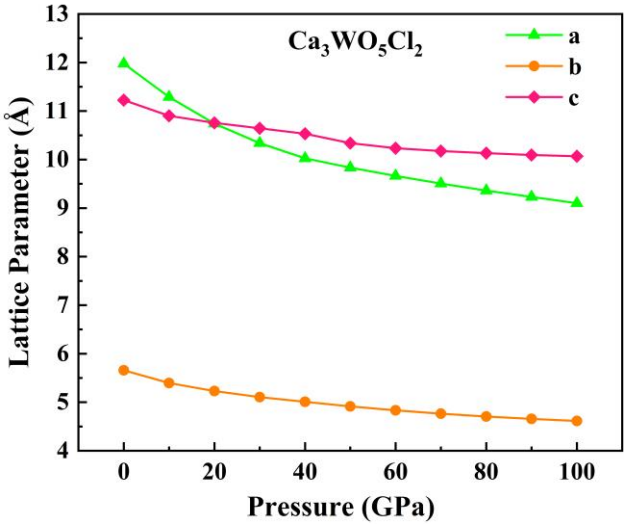

(a)

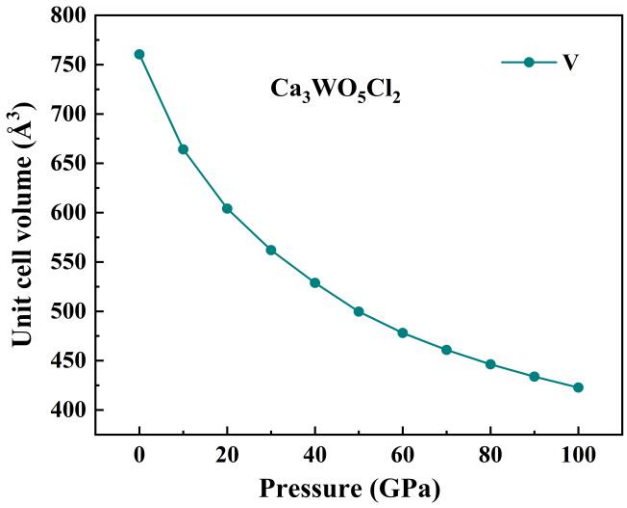

(b)

Fig. 2. Variation of (a) lattice parameters and (b) cell volume with pressure for $Ca_3WO_5Cl_2$ (color online)

Table 1. Lattice parameters and volume of unit cell of $Ca_3WO_5Cl_2$ after geometry optimisation in comparison with literature

a/Å	b/Å	c/Å	V/Å^3	References
11.820	5.587	11.132	735.2	[28]
11.8112	5.5855	11.1265	734.04	[12]
11.8007	5.5574	11.0789	-	[13]
11.9752	**5.6567**	**11.2259**	**760.463**	**This work**

The effects of pressure on the band structure, density of states, and charge density difference of $Ca_3WO_5Cl_2$ have been investigated by calculations. Although the calculation method used (GGA-PBE) tends to underestimate the band gap values [29, 30], the relative values remain meaningful and can be used as a

valid approximation for qualitative analysis of the band structure and density of states. The band structure near the Fermi energy level plays a crucial role in characterising the physical properties of materials. In this study, the band structures near the Fermi energy level of $Ca_3WO_5Cl_2$ were plotted for pressures of 0 GPa, 20 GPa, 50 GPa, and 100 GPa in Fig. 3. The variations of the band gap from 0 to 100 GPa are shown in Fig. 4.

Fig. 3(a) illustrates that in the absence of applied pressure, the valence band maximum (VBM) and conduction band minimum (CBM) of $Ca_3WO_5Cl_2$ are located at the high symmetry point G with a band gap of 3.409 eV, consistent with existing calculations of 3.440 eV [13]. This indicates that $Ca_3WO_5Cl_2$ is a direct bandgap material. Fig. 3(b)(c)(d) show that under increasing pressure, the VBM and CBM of $Ca_3WO_5Cl_2$ approach the Fermi energy level (E_F), while remaining at the G-point position. At 10 GPa pressure, the band gap is 3.43 eV, which is close to the zero-pressure band gap. With increasing applied pressure, the band gap systematically decreases from 3.361 eV at 20 GPa to 2.715 eV at 100 GPa (Fig. 4). These results indicate that hydrostatic pressure is an effective means of controlling the electronic properties of $Ca_3WO_5Cl_2$. However, it does not effectively induce a transition from a direct bandgap to an indirect bandgap.

The total and partial density of states of $Ca_3WO_5Cl_2$ under various hydrostatic pressures are plotted in Fig. 5. In the absence of applied pressure, the valence band density of states near the Fermi energy level is predominantly contributed by the O-2p orbital, with a minor contribution from the Cl-3p. The conduction band density of states near the E_F mainly originates from the W-5d orbital, with a smaller contribution from the O-2p orbital. The blue-green luminescence of $Ca_3WO_5Cl_2$ can be attributed to the charge transfer transition between the valence band O-2p orbital and the conduction band W-5d orbital.

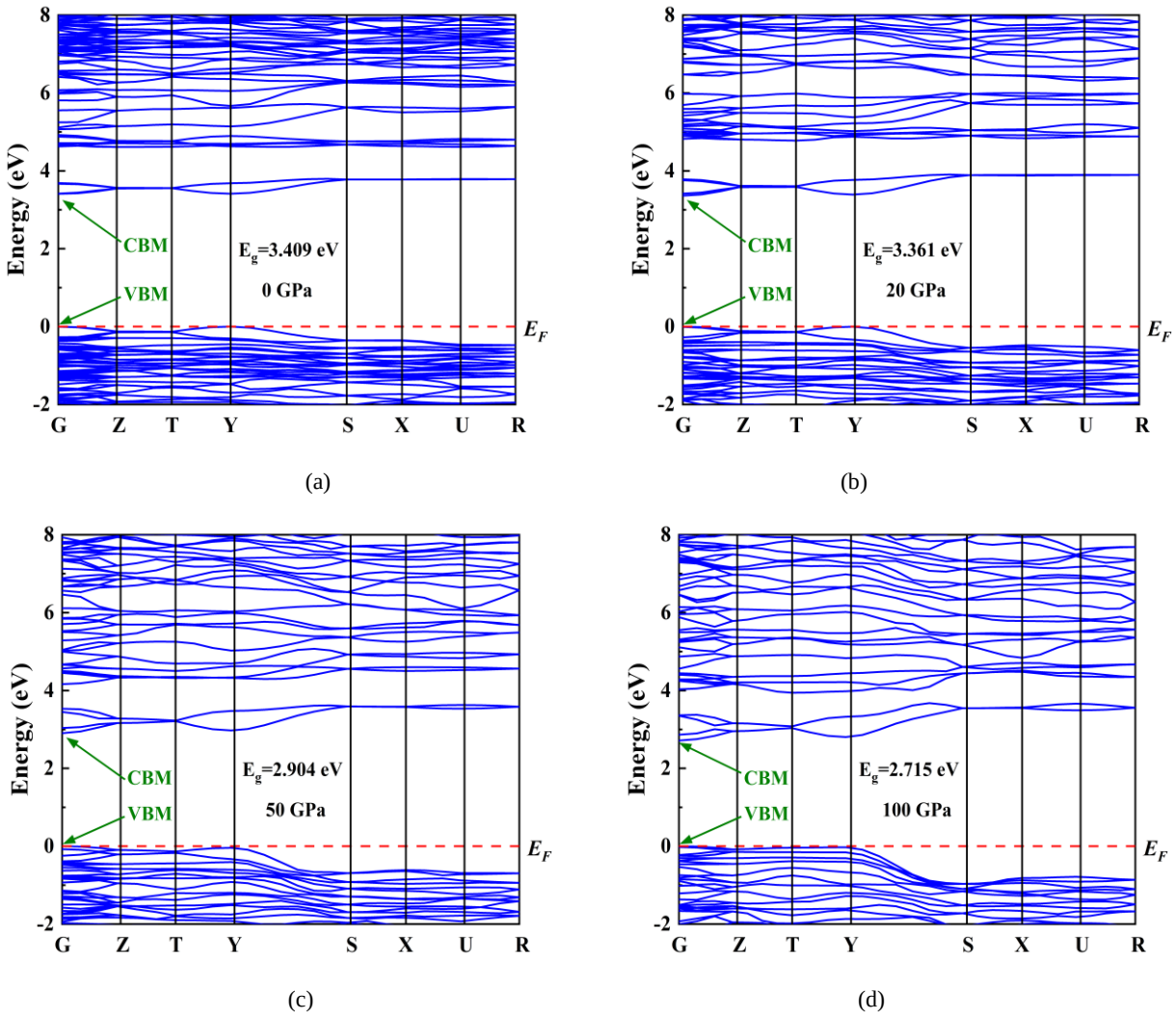

Fig. 3. The band structures of $Ca_3WO_5Cl_2$ at (a) 0 GPa, (b)20 GPa, (c)50 GPa, and (d)100 GPa. The red dashed line indicates the Fermi level (color online)

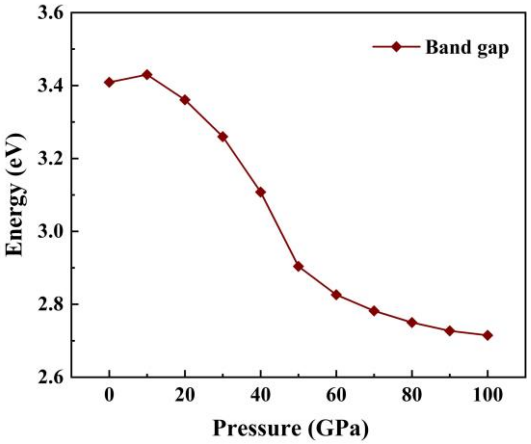

Fig. 4. Band gap of $Ca_3WO_5Cl_2$ under different pressure conditions

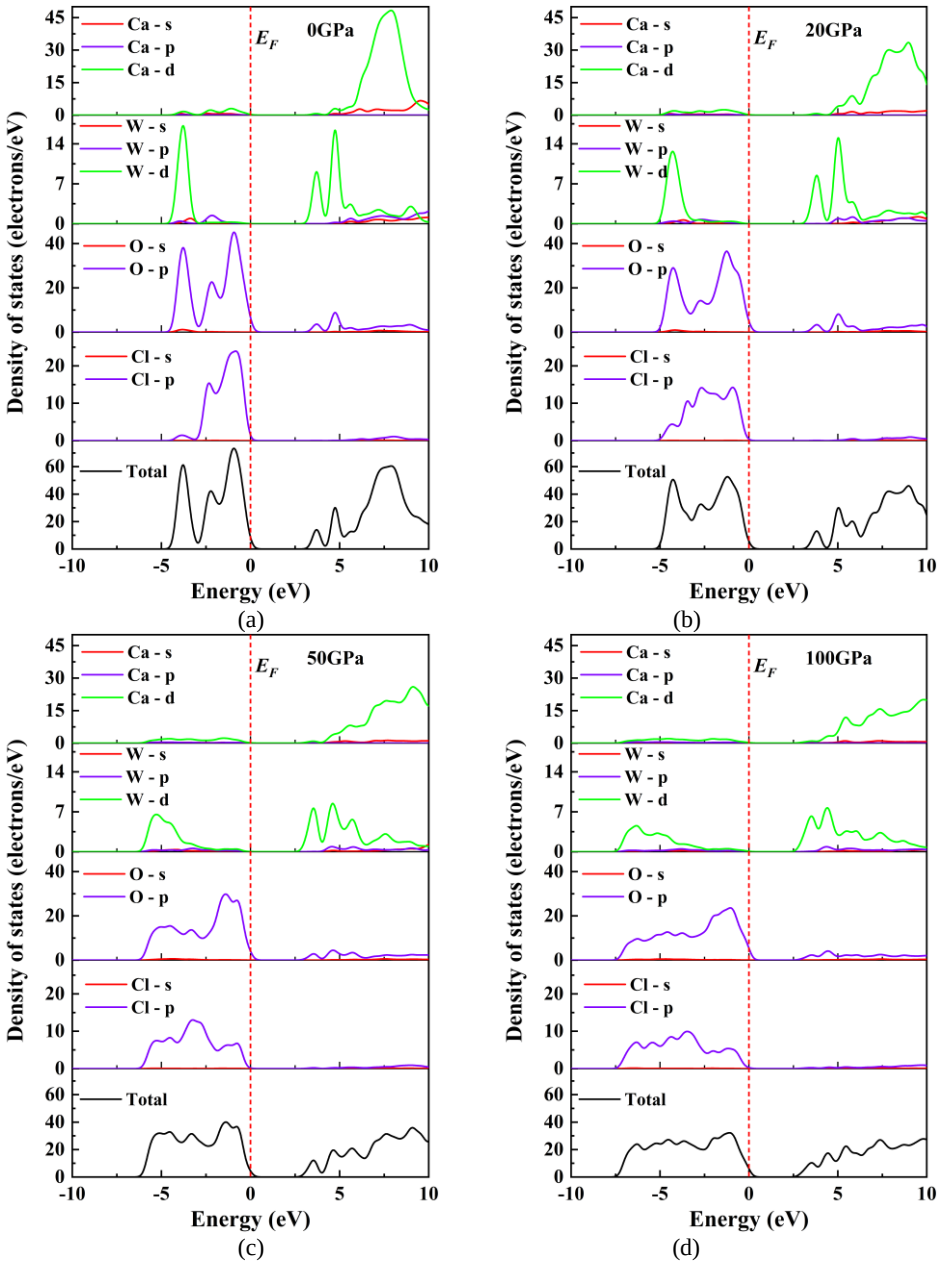

Fig. 5. Density of states of $Ca_3WO_5Cl_2$ under the pressure of (a) 0 GPa, (b) 20 GPa, (c)50GPa, and (d)100GPa. The red dashed line indicates the Fermi level (color online)

The contribution of the Ca atoms to the density of states mainly arises from the Ca-3d orbital in the conduction band; however, the resulting density of states lies above the 5 eV energy level and has minimal contribution near the Fermi energy level. Fig. 5(b), (c) and (d) indicate that the contribution ratio of each atom to the density of states does not vary significantly with applied pressure. However, the density of states is reduced and broadened to varying degrees, which can be attributed to the increased hybridisation between electron orbitals under hydrostatic pressure. Notably, with increasing pressure, the density of states contributed by the W-5d orbitals near 3 eV shifts to lower energy regions, thereby causing the decrease in band gap under pressure.

To examine the details of interatomic charge transfer, the charge density difference of $Ca_3WO_5Cl_2$ at different pressures was calculated. The results are shown in Fig. 6. Comparing the three sets of calculations, it is evident that as the pressure increases, the O atoms gain more electrons while the W atoms lose electrons in the $Ca_3WO_5Cl_2$ crystal. This indicates that the charge transfer in $Ca_3WO_5Cl_2$ can be regulated by pressure.

The optical properties of $Ca_3WO_5Cl_2$ at different hydrostatic pressures have been calculated. The results will help to expand the application range and improve the performance of tungstate in devices. The optical properties of the material in the linear response range can be described by the complex dielectric function:

$$\varepsilon(\omega)=\varepsilon_1(\omega)+i\varepsilon_2(\omega) \tag{1}$$

where $\varepsilon_1(\omega)$, $\varepsilon_2(\omega)$ are the real part of the dielectric function and the imaginary part of the dielectric function, respectively [31]. The imaginary part $\varepsilon_2(\omega)$ can be calculated by the following equation:

$$\varepsilon_2(\omega)=\frac{Ve^2}{2\pi\hbar m^2\omega^2}\int d^3k\sum_{nn'}\left|\langle kn|\boldsymbol{p}|kn'\rangle\right|^2 f(kn) \times\left[1-f(kn')\right]\delta(E_{kn}-E_{kn'}-\hbar\omega) \tag{2}$$

where V is the unit volume, p is the momentum transition matrix, e is the electronic charge, and kn and kn' are the valence band and conduction band wave functions, respectively.

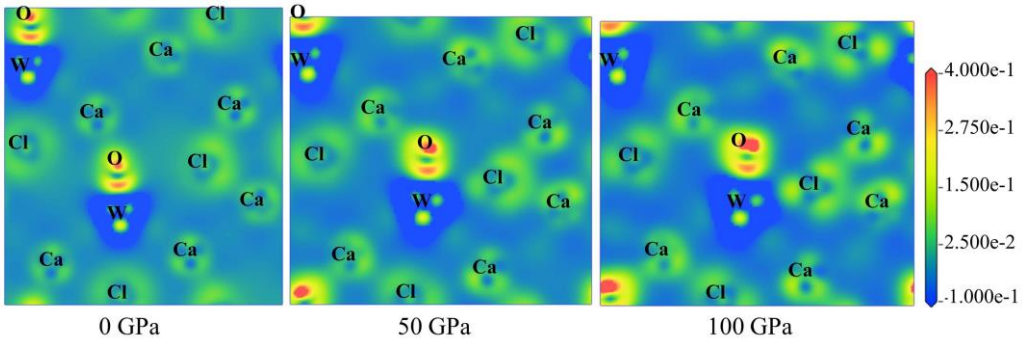

Fig. 6. The charge density difference of $Ca_3WO_5Cl_2$ at 0 GPa, 50 GPa, and 100 GPa (color online)

The real part $\varepsilon_1(\omega)$ can be derived directly from the imaginary part via the Kramers-Kronig transform [32, 33]:

$$\varepsilon_1(\omega)=1+\frac{2}{\pi}M\int_0^{\infty}\frac{\omega'\varepsilon_2(\omega')}{\omega'^2-\omega^2}d\omega' \tag{3}$$

Other optical properties of the material, such as the absorption coefficient $\alpha(\omega)$, reflectivity $R(\omega)$, refractive index $n(\omega)$ and extinction coefficient $k(\omega)$, can be deduced from the dielectric function and are calculated as follows [34-36]:

$$\alpha(\omega)=\sqrt{2\left[\sqrt{\varepsilon_1^2(\omega)+\varepsilon_2^2(\omega)}-\varepsilon_1(\omega)\right]} \tag{4}$$

$$R(\omega)=\left|\frac{\sqrt{\varepsilon_1(\omega)+i\varepsilon_2(\omega)}-1}{\sqrt{\varepsilon_1(\omega)+i\varepsilon_2(\omega)}+1}\right|^2 \tag{5}$$

$$n(\omega)=\sqrt{\frac{\sqrt{\varepsilon_1^2(\omega)+\varepsilon_2^2(\omega)}+\varepsilon_1(\omega)}{2}} \tag{6}$$

$$k(\omega)=\sqrt{\frac{\sqrt{\varepsilon_1^2(\omega)+\varepsilon_2^2(\omega)}-\varepsilon_1(\omega)}{2}} \tag{7}$$

The above equations provide the theoretical basis for analysing the crystal energy band structure and optical properties, which are indicative of the luminescence mechanism and electron transitions between energy levels. A systematic investigation of the

optical properties of $Ca_3WO_5Cl_2$ under high pressure was carried out based on these relationships. The dielectric function curves of $Ca_3WO_5Cl_2$ under pressure modulation are presented in Fig. 7(a) and Fig. 7(b).

Fig. 7(a) illustrates that the real part of the dielectric function, $\varepsilon_1(\omega)$, increases with energy in the low-energy range of 0 eV to 5.09 eV in the absence of pressure, with a slight trough observed at 6.23 eV. In the energy range of 7 eV to 10 eV, $\varepsilon_1(\omega)$ rapidly decreases with increasing energy, corresponding to a significant rise in the absorption coefficient. As the applied pressure increases, $\varepsilon_1(\omega)$ shifts towards higher energies in the range of 0 eV to 10 eV, and the peak gradually rises. This indicates an enhancement in reflectivity and improved reflective properties of light. Fig. 7(b) demonstrates that the imaginary part of the dielectric function, $\varepsilon_2(\omega)$, is more prominently influenced by hydrostatic pressure. At 0 GPa pressure, the peak value of $\varepsilon_2(\omega)$ is 5.74 (8.14 eV). As the pressure increases, $\varepsilon_2(\omega)$ shifts towards higher energies in the range of 8 eV to 20 eV, with an increase in the peak value. At 100 GPa pressure, the peak value of $\varepsilon_2(\omega)$ is 7.38, and its position shifts to 9.44 eV.

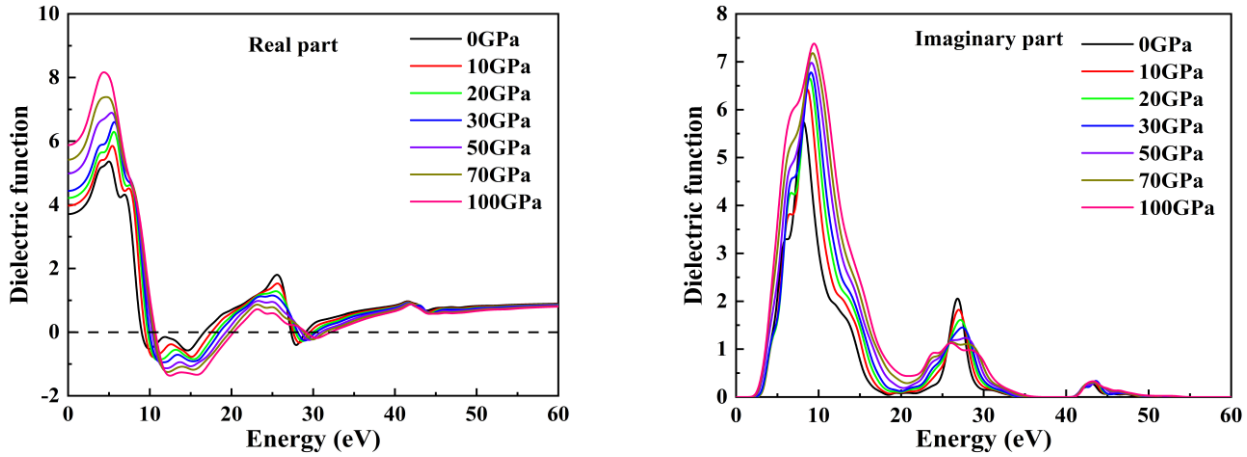

(a) (b)

Fig. 7. (a) Real part of the dielectric function and (b) imaginary part of the dielectric function for $Ca_3WO_5Cl_2$ under pressure (color online)

Fig. 8 presents the absorption coefficient, reflectivity, refractive index, and extinction coefficient of $Ca_3WO_5Cl_2$ at different pressures in the energy range from 0 eV to 60 eV. As observed in Fig. 8(a), the absorption coefficients of $Ca_3WO_5Cl_2$ are zero in the energy range of 0 eV to 1.51 eV, 35.65 eV to 39.60 eV, and 54.58 eV to 60 eV even without applied pressure. Increasing hydrostatic pressure up to 100 GPa does not alter the absorption coefficients within these ranges. Three peaks in the absorption coefficient occur at energy positions of 9.27 eV, 14.22 eV, and 27.47 eV, all within the UV region, indicating the strong absorption capacity of $Ca_3WO_5Cl_2$ for UV light. The absorption coefficients in the energy range of 9.27 eV to 18.53 eV undergo significant shifts towards higher energies with increased pressure, and the absorption coefficients also increase with pressure.

The reflectivity spectra of $Ca_3WO_5Cl_2$ at different pressures are depicted in Fig. 8(b). At zero pressure, $Ca_3WO_5Cl_2$ exhibits three reflectivity peaks at energy positions of 0.3 (9.31 eV), 0.41 (15.88 eV), and 0.33 (28.47 eV), respectively. As the pressure gradually increases from 0 GPa to 100 GPa, the low-energy peak (9.31 eV) increases, while the high-energy peaks (15.88 eV and 28.47 eV) decrease, resulting in a shift of the reflectivity spectrum towards higher energies. The refractive index (n) and extinction coefficient (k) as functions of energy are displayed in Fig. 8(c) and (d), respectively. Both changed significantly with changes in the applied hydrostatic pressure. In the energy range of 0 eV to 10 eV, as the pressure increases from 0 GPa to 100 GPa, the n value shows a clear increase, with the maximum value rising from 2.36 to 2.90. The extinction coefficient, which describes the ability of the substance to absorb light, also exhibits changes. With increasing pressure, the extinction coefficient spectrum in the range of 10 eV to 20 eV shifts towards higher energies, with the peak value increasing from 1.53 (at 0 GPa) to 1.83 (at 100 GPa). Within this energy range, the k value undergoes a rapid decrease, consistent with the change observed in the absorption coefficient.

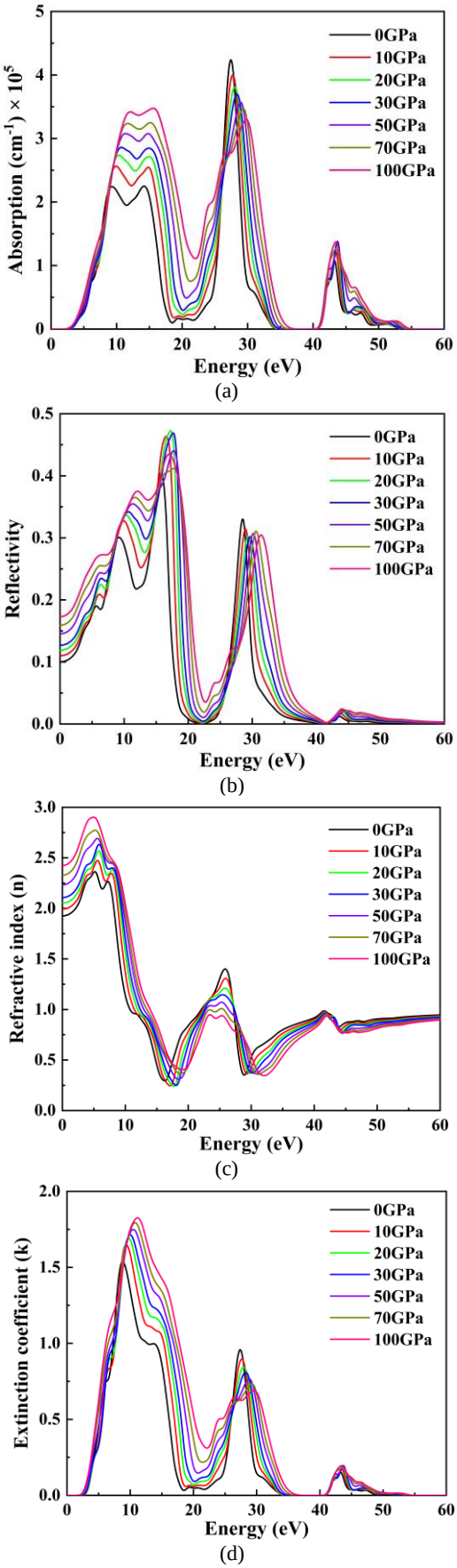

Fig. 8. (a) Absorption coefficient, (b) reflectivity, (c) refractive index and (d) extinction coefficient of $Ca_3WO_5Cl_2$ under pressure (color online)

4. Conclusion

In conclusion, this study has used first-principles calculations based on density functional theory to investigate the electronic structure and optical properties of $Ca_3WO_5Cl_2$ under varying hydrostatic pressures. Analysis of band structure, density of states, dielectric function, absorption coefficient, reflectivity, and complex refractive index provided valuable insight into the pressure modulation behaviour of $Ca_3WO_5Cl_2$. The results demonstrate that hydrostatic pressure induces significant changes in the electronic structure and optical properties of $Ca_3WO_5Cl_2$. Increasing pressure leads to a decrease in lattice parameters, cell volume, and band gap of $Ca_3WO_5Cl_2$. Moreover, the absorption coefficients of $Ca_3WO_5Cl_2$ in the UV region are enhanced under pressure. These findings provide a deeper understanding of the optical properties of tungstates and offer potential avenues for their application in UV protection and energy conversion.

Acknowledgements

This work was supported by the Natural Science Foundation of Jiangsu Higher Education Institutions of China (Grant No.23KJA510005).

References

[1] J. Zhang, Z. Song, P. Cai, X. Wang, Phys. Chem. Chem. Phys. **25**(3), 1565 (2023).
[2] S. Zhang, P. Zhang, Y. Huang, H. J. Seo, J. Lumin. **207**, 460 (2019).
[3] H. Zhou, N. Guo, X. Lü, Y. Ding, L. Wang, R. Ouyang, B. Shao, J. Lumin. **217**, 116758 (2020).
[4] S. Wu, P. Xiong, Q. Liu, Y. Xiao, Y. Sun, E. Song, Y. Chen, Adv. Opt. Mater. **10**(23), 2201718 (2022).
[5] Z. Chen, B. Wang, X. Li, L. Kang, Y. Chen, Y. Chen, H. Sun, Q. Zeng, J. Alloys Compd. **770**, 559 (2019).
[6] M. Rakshita, A. A. Sharma, P. P. Pradhan, K. A. K. Durga Prasad, K. Jayanthi, D. Haranath, Ceram. Int. **49**(11), 16775 (2023).
[7] S. Yang, S. Park, J. Phys. Chem. Lett. **13**(41), 9766 (2022).
[8] T. Hu, H. Lin, Y. Gao, J. Xu, J. Wang, X. Xiang, Y. Wang, J. Am. Ceram. Soc. **101**(8), 3437 (2018).
[9] Y. Zhao, X. Wang, Y. Zhang, Y. Li, X. Yao, J. Alloys Compd. **834**, 154998 (2020).
[10] R. Krishnan, S. G. Menon, D. Poelman, R. E. Kroon, H. C. Swart, Dalton Trans. **50**(1), 229 (2021).
[11] S. Peng, L. Liu, L. Wang, R. Rong, L. Song, W. You, J. Shi, Y. Zhang, J. Rare Earths **40**(9), 1417 (2022).
[12] S. Bi, H. Cheng, M. Luo, P. Cai, L. Qin, Ceram. Int. **49**(11), 18592 (2023).
[13] Y. Kitagawa, S. Takemura, D. Hirai, Z. Hiroi, J.

Ueda, S. Tanabe, Phys. Chem. Chem. Phys. **24**(39), 24203 (2022).
[14] L. Cai, X. Tang, C. Liu, R. Lin, Chin. J. Phys. **57**, 157 (2019).
[15] J. M. Ablett, S.R. Shieh, V. Balédent, J. C. Woicik, E. Cockayne, E. L. Shirley, Phys. Rev. B **104**(5), 054119 (2021).
[16] S. Mahlik, F. Diaz, P. Boutinaud, Opt. Mater. **74**, 41 (2017).
[17] M. D. Segall, P. J. D. Lindan, M. J. Probert, C. J. Pickard, P. J. Hasnip, S. J. Clark, M. C. Payne, J. Phys.: Condens. Matter **14**(11), 2717 (2002).
[18] W. Kohn, L. J. Sham, Phys. Rev. **140**(4), A1133 (1965).
[19] S. J. Clark, M. D. Segall, C. J. Pickard, P. J. Hasnip, M. I. J. Probert, K. Refson, M. C. Payne, Z. Kristallogr. **220**(5-6), 567 (2005).
[20] P. Hohenberg, W. Kohn, Phys. Rev. **136**(3), B864 (1964).
[21] W. Kohn, Rev. Mod. Phys. **71**(5), 1253 (1999).
[22] J. P. Perdew, J. A. Chevary, S. H. Vosko, K. A. Jackson, M. R. Pederson, D. J. Singh, C. Fiolhais, Phys. Rev. B **46**(11), 6671 (1992).
[23] M. C. Payne, M. P. Teter, D. C. Allan, T. A. Arias, J. D. Joannopoulos, Rev. Mod. Phys. **64**(4), 1045 (1992).
[24] J. P. Perdew, K. Burke, M. Ernzerhof, Phys. Rev. Lett. **77**(18), 3865 (1996).
[25] H. J. Monkhorst, J. D. Pack, Phys. Rev. B **13**(12), 5188 (1976).
[26] B. G. Pfrommer, M. Côté, S. G. Louie, M. L. Cohen, J. Comput. Phys. **131**(1), 233 (1997).
[27] T. H. Fischer, A. Jan, J. Phys. Chem. **96**(24), 9768 (1992).
[28] Z. Zikmund, Acta Cryst. B **30**(11), 2587 (1974).
[29] J. P. Perdew, M. Levy, Phys. Rev. Lett. **51**(20), 1884 (1983).
[30] M. Ullah, R. Neffati, G. Murtaza, S. Khan, M. Haneef, M. W. Ashraf, Mater. Sci. Semicond. Process. **150**, 106977 (2022).
[31] J. Han, D. Xu, M. Yang, F. Tian, Mater. Sci. Semicond. Process. **144**, 106566 (2022).
[32] W. Zhou, A. N. Rudenko, S. Yuan, Adv. Electron. Mater. **6**(1), 1900860 (2019).
[33] S. Saha, T. P. Sinha, A. Mookerjee, Phys. Rev. B **62**(13), 8828 (2000).
[34] J. El Hamdaoui, M. El-Yadri, M. Farkous, M. Kria, M. Courel, M. Ojeda, L. M. Perez, A. Tiutiunnyk, D. Laroze, E. M. Feddi, Nanomaterials **11**(10), 2692 (2021).
[35] M. Gandouzi, Z. R. Khan, A. S. Alshammari, Comput. Mater. Sci. **156**, 346 (2019).
[36] H.-C. Huang, C.-L. Yang, M.-S. Wang, X.-G. Ma, Spectrochim. Acta, Part A **208**, 65 (2019).

*Corresponding author: xfwang@njupt.edu.cn